The P-O bond lengths in vitreous P_2O_5 probed by neutron diffraction with high real-space resolution

1998 J. Phys.: Condens. Matter 10 261

(http://iopscience.iop.org/0953-8984/10/2/004)

J. Phys.: Condens. Matter **10** (1998) 261–270. Printed in the UK PII: S0953-8984(98)80988-0

The P–O bond lengths in vitreous P_2O_5 probed by neutron diffraction with high real-space resolution

U Hoppe†, G Walter†, A Barz‡, D Stachel‡ and A C Hannon§

† Department of Physics, Rostock University, Rostock D-18051, Germany
‡ Otto Schott Institute, Friedrich Schiller University Jena, Jena D-07743, Germany
§ ISIS Facility, Rutherford Appleton Laboratory, Chilton, Didcot OX11 0QX, UK

Received 15 January 1997, in final form 30 September 1997

Abstract. Neutron diffraction has been used to determine the two P–O bond lengths which occur in the threefold-linked tetrahedral PO_4 structural units of vitreous P_2O_5. The large maximum momentum transfer ($Q_{max} \approx 500$ nm^{-1}) which is available on the LAD instrument at the ISIS spallation neutron source gives high real-space resolution which enables a clear separation to be made between P–O bond lengths involving terminal oxygens (143.2 ± 0.5 pm) and those involving bridging oxygens (158.1 ± 0.3 pm). The two P–O distances in vitreous P_2O_5 were found to have narrower distributions than have previously been observed, using the same experimental conditions, for any other modified phosphate glass.

1. Introduction

Phosphorus may be said to be the strongest network former in oxide systems in view of the fact that it has an electric field strength at the position of the neighbouring oxygen which is larger than for any other cation [1]. However, vitreous (v-)P_2O_5 is extremely hygroscopic, making it difficult both to prepare and to keep water free during an experiment, and consequently it has been the subject of very few structural studies.

Spectroscopic investigations [2–6] have shown that v-P_2O_5 is formed of corner-sharing PO_4 tetrahedra, as is the case for all other phosphate glasses. One of the four vertices of the PO_4 unit in v-P_2O_5 is occupied by a terminal oxygen atom (O_T) as a consequence of the fivefold valency of phosphorus, whilst the other three vertices are occupied by bridging oxygens (O_Bs) which are bonded to the rest of the network. The P–O bond length for the terminal oxygen is expected to be smaller than for the bridging oxygens because it is doubly bonded. The two types of P–O bond are illustrated by figure 1 which shows a section of the P_2O_5 network. The bond lengths in the glassy system are expected to be similar to those in the three crystalline polymorphs of P_2O_5, as recently determined [7–9]. Values for the length of the bond to the terminal oxygen range from 143.1 to 145.2 pm, whilst the values for the bridging oxygens range from 156.2 to 159.7 pm. By use of *ab initio* molecular orbital calculations on a small cluster of two linked PO_4 tetrahedra, Uchino and Ogata [10] obtained lengths of 143.9 and 157.7 pm for the two types of bond. However, until now a successful experimental separation of the two P–O distances in v-P_2O_5 has not been reported. A knowledge of the P–O_T and P–O_B bond lengths is required in order to describe the exact geometry of the PO_4 unit in v-P_2O_5, and a determination of these values is the aim of the present study.

0953-8984/98/020261+10$19.50

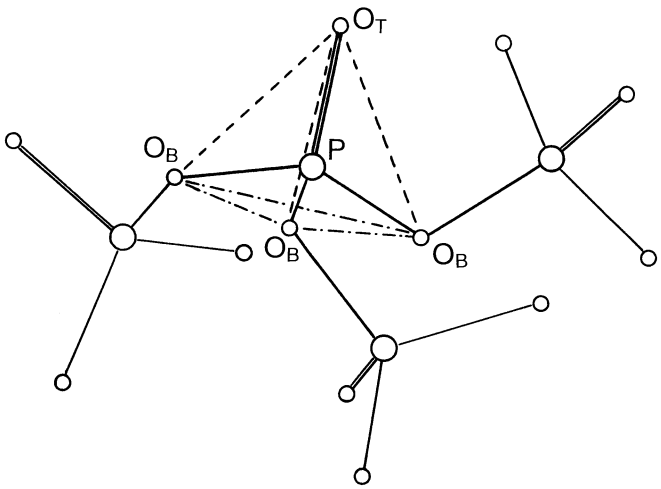

Figure 1. The threefold-linked PO_4 tetrahedron which composes the network of v-P_2O_5. O_T is the double-bonded terminal oxygen atom, O_B is the bridging oxygen. Full lines mark the bonds. The dashed edges of the PO_4 unit are O_B–O_T distances; the dash–dot edges are O_B–O_B distances.

A diffraction experiment which uses the epithermal neutrons produced by a spallation neutron source yields very high real-space resolution. A series of such studies on various phosphate glasses has shown this method resolving the split peak of the P–O bond lengths in the correlation function [11–15].

Wright *et al* [16] have previously reported a measurement of the diffraction pattern of v-P_2O_5 at low to medium Q ($Q_{max} \approx 240$ nm^{-1}), made at a reactor source of neutrons. The data were compared with the diffraction patterns of various single-component network glasses, leading to the conclusion that the medium-range structure of v-P_2O_5 can be related to that of v-As_2O_3; both glasses involve threefold-linked structural units: PO_4 tetrahedra in v-P_2O_5 and AsO_3 pyramids in v-As_2O_3.

2. Experimental procedure

The sample preparation of vitreous P_2O_5 is described elsewhere [6]. The mass density of 2.445 g cm^{-3} used in the data evaluation was taken from an extrapolation of the densities of series of MeO–P_2O_5 glasses (Me = Mg [17], Me = Zn, Ca, Ba [18]). The most serious requirement which concerns the raw materials (P_4O_{10} powder) and the full process of preparation is the absence of any humidity. It is the advantage of neutron diffraction that any contamination with water which could essentially change the structure remarkably increases the incoherent scattering. Thus, a bad sample would be identified immediately. The experiment was performed by use of the liquids and amorphous diffractometer (LAD) at the ISIS Facility of the Rutherford Appleton Laboratory, UK. For the transport, the grain-shaped glassy material was contained in a sealed ampoule. Just before the measurement the sample material was loaded under dry conditions into a thin-walled and leak-tight vanadium cylinder of 11 mm in diameter. During the measurement, the sample container was positioned in the vacuum chamber of the diffractometer. The duration of the data collection of the sample run was 10 hours.

An effective density for the subsequent attenuation and multiple-scattering correction, which is smaller than the density of the compact material, was determined by weighing the container filled with the glass grains. The transmission of the sample measured versus neutron wavelength was used to determine the wavelength-dependent cross-section $\sigma(\lambda)$ which is used to calculate the absorption and the multiple-scattering corrections. A significant water contamination would also be apparent in this measured cross-section $\sigma(\lambda)$ due to the very large incoherent cross-section of hydrogen. The data corrections were performed by use of the ATLAS suite [19] which is available at the ISIS Facility. The curves measured on the 14 detector groups at scattering angles of 5°, 10°, 20°, 35°, 58°, 90°, and 150°, on the left-hand and the right-hand sides of the beam, were corrected separately which finally leads to 14 differential scattering cross-sections extending over different Q-intervals and still affected by inelasticity effects.

According to the nominal composition of the sample the self-scattering was calculated using the approach of Powles [20] and of Howe *et al* [21] for taking into account the inelastic scattering. Since, however, the energy-dependent scattering law of the sample under investigation is not known, the dynamic behaviour of a perfect gas is usually exploited (Placzek [22]). This assumption is quite good in the high-energy range, i.e. for wavelengths of incident neutrons less than about 0.12 nm [23]. Thus, the inelasticity correction can be made properly even for the high-Q data for the large scattering angles.

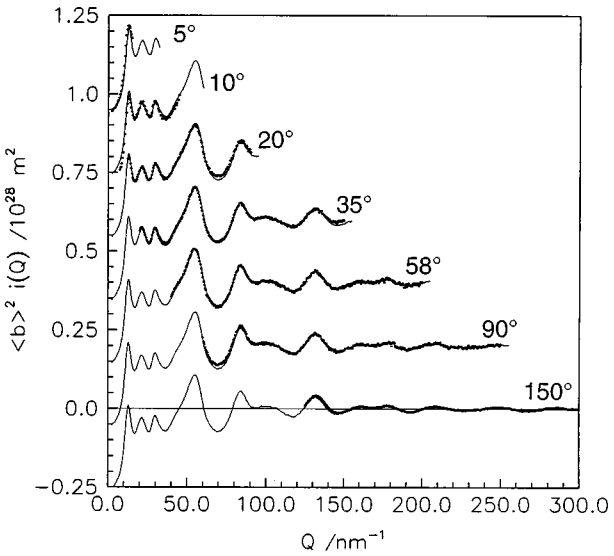

Figure 2. The normalized interference functions of the seven detector groups (dots) showing the different contributions to the final interference function (lines). The upper curves were shifted by 0.2 to improve the clarity of the plot.

An absolute calibration with regard to the vanadium run is not totally successful due to uncertainties in calculating the number of atoms in the neutron beam and viewed by the detector as a consequence of the powder packing of the coarse-grained sample. Due to the small Q-range in the case of the smaller scattering angles, the correct factor for adjusting the experimental curves to the self-scattering terms cannot be obtained directly. Hence, the normalization starts with the calibration of the differential scattering cross-sections of the 150° detector where a large Q-range from 150 nm^{-1} to up 500 nm^{-1} can be used to

Table 1. Parameters of the Gaussian curves used in the fit of the P–O and O–O distance peaks. The distances r_{ij} and the root mean square displacements l_{ij} are given in pm.

Atom pair	Coordination number	Distance r_{ij}	rmsd l_{ij}
$P–O_T$	0.90(10)	143.2(5)	2.8(4)
$P–O_B$	3.05(10)	158.1(3)	3.9(3)
O–O	1.75(10)*	244(2)	6.0(8)
	2.95(10)*	257(1)	6.8(9)

* 4.8 is the expected O–O coordination number of threefold-linked PO_4 units [14, 17].

determine the adjustment factor. Subsequently, the self-term which includes the incoherent scattering was subtracted from the normalized differential scattering cross-sections. The resulting function $\langle b\rangle^2 i(Q)$ is plotted in figure 2 where $\langle b\rangle$ is the mean of the scattering lengths. $i(Q)$ stands for the interference function which is the total Faber–Ziman structure factor, $a_{FZ}(Q)$, as given by Waseda [24], diminished by unity ($i(Q) = a_{FZ}(Q) - 1$). One after another, the curves of the other detectors were adjusted, every time checking the agreement with the curves measured at the higher angles. The inelasticity correction becomes negligible for small scattering angles. At small Q-values the portion of elastic scattering in solids is large. Except of some unrealistic features in the curves of the detectors at angles $58^\circ, 90^\circ$ and 150° on one side of the diffractometer, all of the normalized curves from both sides could be well combined. The results are shown in figure 2. The high-Q part of $i(Q)$ becomes more visible if the function is weighted by Q (compare figure 4(a)—see later).

3. Results

Figure 3 shows the real-space correlation function, $T(r)$, of v-P_2O_5 in the region of the first-neighbour distances. $T(r)$ was obtained by Fourier transformation of $Qi(Q)$ with an upper integration limit Q_{max} of 500 nm^{-1} and not using any modification function. There are two clear P–O contributions to $T(r)$ and the second component is three times larger than the first. This result is consistent with the formation of threefold-linked PO_4 units discussed in the introduction. The two peak components were fitted by Gaussian curves whose parameters are given in table 1. The truncation effect of the Fourier transformation was taken into account in the fit by folding the model peaks with the appropriate peak functions as was described in reference [14]. The truncation effect leads to the occurrence of small ripples and a peak broadening. However, the broadening effect is very small due to the large value of Q_{max}. A good fit of the O–O distance peak which corresponds to the edges of the PO_4 tetrahedron was only possible in approximating the peak by two Gaussian curves. The corresponding parameters are listed in table 1. The unfolded model functions are shown in the lower part of figure 3.

At this point we will consider the influence of hydrogen on the results obtained in a time-of-flight experiment. When a fixed-wavelength neutron diffraction experiment is performed using a reactor source of neutrons a single diffraction pattern is measured as a function of the scattering angle 2θ. It is thus relevant to consider the behaviour of the inelasticity effect on the self-scattering as a function of 2θ only. However, for a pulsed neutron diffraction experiment, spectra are recorded at several different fixed angles 2θ as a function of momentum transfer Q ($=4\pi \sin\theta/\lambda$). Hence it is necessary to consider the

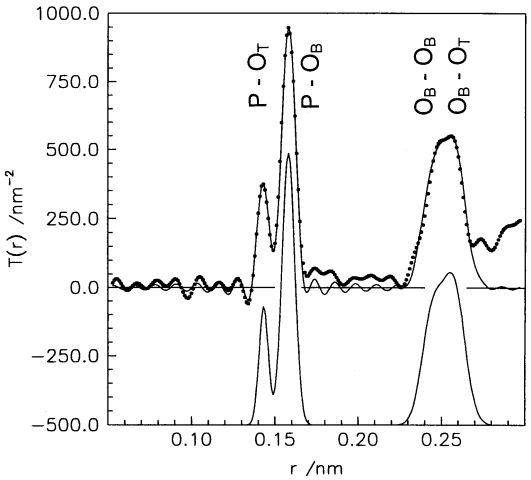

Figure 3. The real-space correlation function, $T(r)$, of v-P_2O_5 showing the P–O bond distances at about 0.150 nm and the O–O peak. The experimental curve is given by dots. The solid line marks the fitted model peaks obtained after folding them with the appropriate peak functions which take into account the truncation effect of the Fourier transformation. The original Gaussian peaks for which parameters are given in table 1 are plotted in the lower part.

behaviour of the inelasticity effect as a function of both 2θ and Q. For a fixed scattering angle 2θ the self-scattering is found to rise very strongly at low Q, which is quite unlike the droop at high 2θ that is observed for a fixed-wavelength experiment. This is a result of the different integration paths in Q–E space for the two types of diffraction experiment. The rise at low Q is much more severe for a detector at high scattering angle than for a detector at low scattering angle (and in this way the inelasticity effect is more severe for larger 2θ in both fixed-wavelength and time-of-flight neutron diffraction experiments). Figure 6 of reference [19] shows this type of behaviour in detail whilst reference [25] shows an example of the kind of results that may be expected for a sample containing a significant amount of hydrogen. Hydrogen has a very large incoherent neutron scattering cross-section and also it shows a very strong inelasticity effect as a result of its light mass. Thus pulsed neutron diffraction is especially sensitive to the presence of hydrogen in a sample in even quite small concentrations (say $\sim$1 at.%).

The experimental data on v-P_2O_5 were examined carefully for any sign of water contamination. As discussed above, the presence of hydrogen in the sample would give rise to a strong rise at low Q in the measured data which would be much more pronounced for a detector at high angle than one at low angle. As can be seen from the results in figure 2, no such sign of water contamination was observed. In addition, the total cross-section, $\sigma(\lambda)$, measured (cf. section 2) does not indicate any significant contamination with water.

The weighted interference function, $Qi(Q)$, of the experimental data is plotted in figure 4(a). This function was chosen for presentation of the scattering result because it accentuates the oscillations at high Q. Beyond $Q > 550$ nm^{-1} the noise makes it meaningless to exploit the data. The high-Q part of the scattering curve contains only information about the first-neighbour distances. In order to illustrate this situation the contributions of the P–O bonds and the O–O distances to the $Qi(Q)$ function are plotted in figure 4(b). Here the parameters of table 1 were used in

$$Qi_{ij}(Q) = [(2-\delta_{ij})c_i b_i b_j/\langle b\rangle^2]N_{ij}(\sin(r_{ij}Q)/r_{ij})\exp(-Q^2 l_{ij}^2/2) \qquad (1)$$

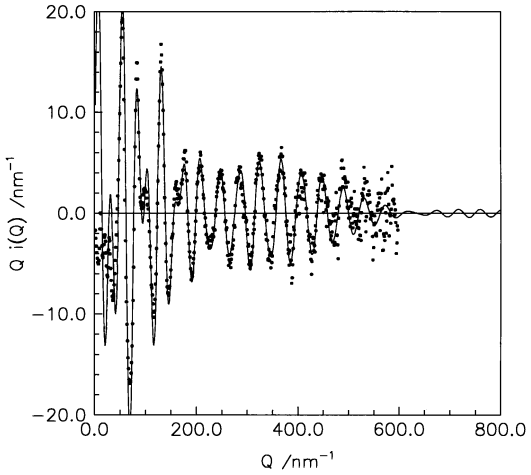

(a)

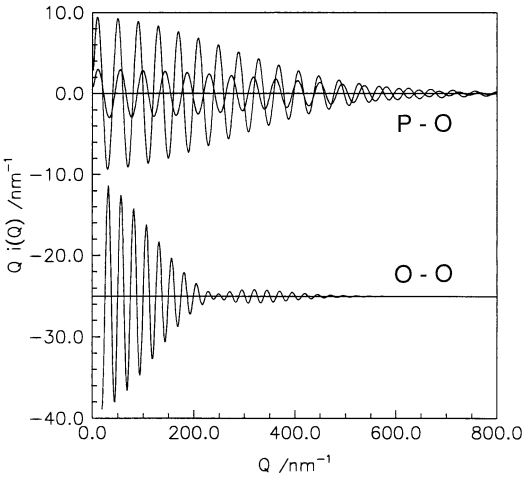

(b)

Figure 4. The weighted interference function, $Qi(Q)$, of v-P_2O_5. (a) The experimental curve is given by dots. The solid line represents the curve which is obtained by superimposing the contributions of the various P–O and the O–O model peaks whose parameters are given in table 1. (b) The two contributions of the P–O bonds are given separately in the upper part. The model function of the total O–O peak, shifted for clearness, is found in the lower part.

where c_i and b_i are the molar fraction and the scattering length of the atomic species i. δ_{ij} stands for the Kronecker symbol. N_{ij} is the number of atoms j distant from an atom i by r_{ij}. The root mean square deviation, l_{ij}, of this distance corresponds to the fwhm Δr_{ij} of the Gaussian curve via $l_{ij} = 0.425\Delta r_{ij}$. The model functions $Qi(Q)$ are shown for each of the two P–O bonds separately. Their superposition leads to amplified (420 nm^{-1}) and to reduced (at $Q = 210$ and 630 nm^{-1}) oscillations in the total $Qi(Q)$ curve (figure 4(a)). The O–O distance peak clearly deviates from that of a single-Gaussian peak (figure 3) but it is not well resolved into those two peaks which were used in the fit. The minimum of the O–O contribution to $Qi(Q)$ at 250 nm^{-1} and its relatively weak magnitude beyond this

point (cf. figure 4(b)) arise from this splitting, and it is thus apparent that the measurement of data for Q-values beyond this value was necessary for the observation of this behaviour of the O–O peak.

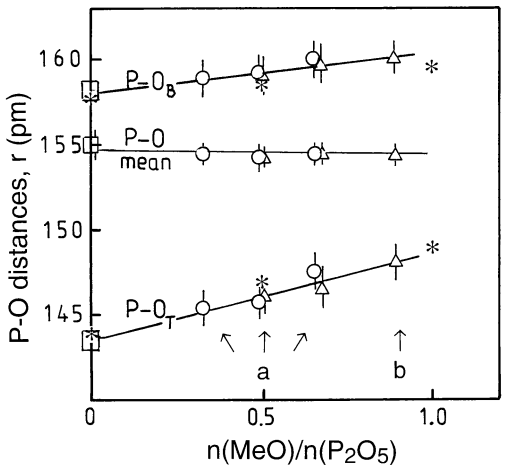

Figure 5. Comparison of the values of the P–O_T and the P–O_B bond lengths of v-P_2O_5 (squares) with those of phosphate glasses modified by different amounts of CaO (circles) and ZnO (triangles). The lines are guides to the eye. The asterisks are theoretical values taken from *ab initio* calculations [10]. The letter (a) denotes values taken from [14, 15]; the values (b) are given in [12].

4. Discussion

The two P–O distances for v-P_2O_5 reported above are highly consistent with the behaviour of distances previously observed in phosphate glasses [12, 14, 15], as is apparent in figure 5 which shows the behaviour of the P–O_T and P–O_B bond lengths. Reference [14] shows an earlier version of this figure without the data for pure v-P_2O_5. The composition dependence of the two bond lengths is indicated by the straight-line guides to the eye. Our x-ray diffraction studies have already shown that the mean P–O bond length does not change as modifier oxide is added to v-P_2O_5 [17, 18]; from the present results of figure 5 it is clear that even though both bond lengths increase as the modifier is added, the mean bond length does not change due to the increasing occurrence of the shorter bond length. This behaviour is in agreement with the *ab initio* molecular orbital calculations of Uchino and Ogata [10], who considered a pair of linked PO_4 units where the outer bridging oxygens were terminated by hydrogen atoms and the appropriate number of the O_T have Na^+ neighbours. As shown in figure 5, their predicted P–O distances agree well with our results. Also the known crystals in this range of composition show the same changes in their P–O bond lengths [14].

A simple mechanism may be used to explain the observed change with composition in the P–O_T bond length by first considering a v-P_2O_5 network composed of threefold-linked units (sometimes known as Q^3-groups). When metal oxide MeO is added, these units are progressively replaced by twofold-linked tetrahedra (Q^2-groups) until the equimolar composition MeO–P_2O_5 is reached. In such a metaphosphate glass the double-bond character is shared between the two P–O_T bonds of the Q^2-group [3] with the result that the P–O_T bond length will be larger than that in a Q^3-unit of v-P_2O_5. The mean P–O_T bond

distance in ultraphosphate networks which contain a mixture of Q^3 and Q^2 is an average of the values for the two groups, weighted according to their relative concentrations and thus, as MeO is added, the observed P–O_T distance increases due to the growing fraction of Q^2-units. The small width of the P–O_T distance peak for ultraphosphate glasses [14, 15] suggests that the P–O_T bond lengths of those Q^3- and Q^2-groups which coexist in the network are equalized.

Table 2. The P–O bond lengths and the number densities of atoms in v-P_2O_5 and in three related crystalline forms. The P–O–P bridging angles and the values N_{OT-O}, which are the numbers of adjacent oxygen atoms of an O_T in other PO_4 tetrahedra at distances of about 310 pm, are correlated with the other values (see the text).

System	Number density of atoms (nm^{-3})	Bond lengths (pm) P–O_T	Bond lengths (pm) P–O_B	N_{OT-O}	P–O–P angle	Reference
P_4O_{10}	67.6	143.2	159.0	4.5	123°	[7]
v-P_2O_5	72.6	143.2	158.1	—	—	This work
P_2O_5 II	80.3	144.5	157.6	8	131°	[8]
P_2O_5 III	87.0	144.4	157.0	10	144°	[9]

Table 2 gives a comparison of the P–O bond lengths and the atomic number density of v-P_2O_5 with the three crystalline forms [7–9]. Although the differences are small, it is clear that the variations in the P–O_T bond lengths correlate with the atomic number density. Thus the geometry of the PO_4 unit depends on the compactness of the network structure. The number of oxygen neighbours of the O_T in other tetrahedra at distances of about 0.31 nm varies from 4.5 in P_4O_{10} [7] up to 10 in P_2O_5 III [9] which should have an effect on the P–O_T bond length. The large P–O_B distances in crystalline P_4O_{10} should result from the small P–O–P bridging angles in the P_4O_{10} molecule. These findings suggest that the network structure of v-P_2O_5 possesses open O_T environments like those in P_4O_{10}, but P–O–P angles rather similar to those in the orthorhombic forms II and III.

A further facet of the PO_4 unit in v-P_2O_5 is the formation of very narrow distance peaks for both P–O bonds. Considering the modified phosphate glasses studied before [11–15] only the l_{ij} of a KPO_3 glass (3.4 pm and 4.7 pm) [13] are comparable with those of v-P_2O_5 (cf. table 1). In pure P_2O_5 the difference between the strong P–O bond energies and the comparatively weak interactions of the O_T atoms with unlinked PO_4 tetrahedra is large. Thus, the outer strain on the P–O bonds is small in such networks of threefold-linked units. The addition of network modifiers causes some more strain on the P–O bonds whereby the influence of K^+ cations is still small. On the other hand, Raman scattering has shown [3] that the band complex of the ν(P=O) mode of the Q^3-group in v-P_2O_5 is broader than the band complex of the ν_s(P–O_2) mode of the Q^2-group in $NaPO_3$ glass. This seems to contradict our observation of the narrow P–O distance peaks in v-P_2O_5.

The fit of the O–O distance peak for modified phosphate glasses [11–15] did not require the use of two Gaussian curves as in the case of v-P_2O_5. Obviously, narrow P–O_T and P–O_B distance peaks and narrow distributions of the O–P–O angles in the tetrahedral PO_4 unit of v-P_2O_5 make the O_B–O_T edge distances shorter than the O_B–O_B edge distances. In figure 1 these edges are marked differently. Using the bond lengths found from the fit (cf. table 1) and the perfect tetrahedral angle of 109.34°, two O–O distances of 245 pm and 258 pm have been calculated. Such lengths match the O–O distances which were found from the fit. However, consideration of the PO_4 tetrahedra in the P_2O_5 crystals, e.g. in P_4O_{10} [7], reveals another situation. The O_B–P–O_T angles are equal to 116° whilst the O_B–P–O_B angles are

equal to 102°. Obviously, the additional negative charge on the P=O double bond causes the P–O_B bonds to move together. Thus, the shorter distances should belong to the O_B–O_B edges as indicated in figure 3. In this paper we have described data which extend up to 550 nm^{-1}, one of the highest ever values of Q_{max} to be reported in any diffraction study, and there seems little prospect of Q_{max} being increased meaningfully in any future diffraction experiment on v-P_2O_5: in addition to the usual problems of the Debye–Waller factor, Q-resolution and decreasing count rate, a possible extension to a higher Q_{max} would have to compete against the cancellation of P–O_T and P–O_B terms which occurs for $Q \simeq 630$ nm^{-1} (cf. figure 4(a)).

The next step in exploring v-P_2O_5, the investigation of the P–O–P bridging angles, however, needs the knowledge of both the P–O_B and the P–P distances. The latter of these lengths will be favourably obtained by the use of an x-ray diffraction experiment. Such work, as well as the modelling of the three-dimensional network of v-P_2O_5, is in progress.

5. Conclusions

The two P–O bond lengths in the PO_4 tetrahedron (which is the threefold-linked unit of the network structure of v-P_2O_5) have been determined. The large Q-range ($Q_{max} \simeq 500$ nm^{-1}) in the neutron diffraction experiment allowed the P–O distance peak to be separated into the components due to the terminal and bridging oxygens with lengths of (143.2 ± 0.5) pm and (158.1 ± 0.3) pm, respectively. The values of the two P–O bonds which were found from the present experiment are highly consistent with the corresponding distances observed previously in some modified phosphate glasses. In these modified phosphate glasses the mean of the P–O distances does not change whilst the P–O_T and P–O_B lengths increase with growing MeO content. The two P–O distance peaks in v-P_2O_5 were found to be narrower than those of other phosphate glasses which have previously been studied under the same experimental conditions. Moreover, for v-P_2O_5 only, the O–O peak which corresponds to the edges of the tetrahedral PO_4 unit seems to be composed from two different distances. It is suggested that they belong to the different O_B–O_T and O_B–O_B edges.

Acknowledgment

Financial support from the Deutsche Forschungsgemeinschaft (Grant WA 842/1-2) is gratefully acknowledged.

References

[1] Dietzel A 1942 *Z. Elektrochem.* **48** 9
[2] Galeener F L and Mikkelsen J C 1979 *Solid State Commun.* **30** 505
[3] Brow R K, Tallant D R, Hudgens J J, Martin S W and Irwin A D 1994 *J. Non-Cryst. Solids* **177** 221
[4] Hudgens J J and Martin S W 1993 *J. Am. Ceram. Soc.* **76** 1691
[5] Meyer K, Hobert H, Barz A and Stachel D 1994 *Vibr. Spectrosc.* **6** 323
[6] Meyer K, Barz A and Stachel D 1995 *J. Non-Cryst. Solids* **191** 71
[7] Jansen M and Luer B 1986 *Z. Kristallogr.* **177** 149
[8] Arbib El H, Elouadi B, Chaminade J P and Darriet J 1996 *J. Solid State Chem.* **127** 350
[9] Stachel D, Svoboda I and Fuess H 1995 *Acta Crystallogr.* C **51** 1049
[10] Uchino T and Ogata Y 1995 *J. Non-Cryst. Solids* **181** 175
[11] Suzuki K and Ueno M 1985 *J. Physique* **46** C8 216
[12] Hoppe U, Walter G, Stachel D and Hannon A C 1995 *Z. Naturf.* a **50** 684
[13] Hoppe U, Walter G, Stachel D and Hannon A C 1996 *Z. Naturf.* a **51** 179

[14] Hoppe U, Walter G, Stachel D, Barz A and Hannon A C 1997 *Z. Naturf.* a **52** 259
[15] Hoppe U, Walter G, Kranold R, Stachel D, Barz A and Hannon A C 1997 *Physica* B **234–236** 388
[16] Wright A C, Hulme R A, Grimley D I, Sinclair R N, Martin S W, Price D L and Galeener F L 1991 *J. Non-Cryst. Solids* **129** 213
[17] Hoppe U, Walter G and Stachel D 1990 *Silikattechnik* **41** 227
[18] Hoppe U, Walter G, Kranold R, Stachel D and Barz A 1995 *J. Non-Cryst. Solids* **192–193** 28
[19] Hannon A C, Howells W S and Soper A K 1990 *Neutron Scattering Data Analysis 1990 (Inst. Phys. Conf. Ser. 107)* ed M W Johnson (Bristol: Institute of Physics Publishing) p 193 ff
[20] Powles J G 1978 *Mol. Phys.* **36** 1181
[21] Howe M A, McGreevy R L and Howells W S 1989 *J. Phys.: Condens. Matter* **1** 3433
[22] Placzek G 1952 *Phys. Rev.* **86** 377
[23] Hoppe U 1986 *Phys. Status Solidi* b **137** K5
[24] Waseda Y 1980 *The Structure of Non-crystalline Materials* (New York: McGraw-Hill) p 11 ff
[25] Bellisent R, Menelle A, Howells W S, Wright A C, Brunier T M, Sinclair R N and Jansen F 1989 *Physica* B **156–157** 217